applied sciences

MDPI

Article

Preparation and Physicochemical Properties of Tannin-Immobilized Membrane Adsorbent

Wei Luo [1], Huiting Lin [1], Zhihao Wu [1], Jingteng Chen [1], Ruiyang Chi [1], Xiaoxia Ye [1,*] and Jie Chen [2,*]

[1] Fujian Provincial Engineering Research Center of Rural Waste Recycling Technology, Department of Environmental Science and Engineering, Fuzhou University, Fuzhou 350108, China; luowei@gdut.edu.cn (W.L.); n190627039@fzu.edu.cn (H.L.); 200627077@fzu.edu.cn (Z.W.); n190627022@fzu.edu.cn (J.C.); 200620062@fzu.edu.cn (R.C.)

[2] College of Environmental and Safety Engineering, Fuzhou University, Fuzhou 350108, China

* Correspondence: yexiaoxia@fzu.edu.cn (X.Y.); jiechen@fzu.edu.cn (J.C.)

Abstract: Plant tannins have the ability to form stable complexes with metal ions, while microporous membranes have low pressure drop and high flux characteristics. Combining these two materials, a new type of tannin-immobilized membrane (M-TAN) adsorption material has been developed. The PA-BWT, PVDF-BWT, CELL -BWT, and PA-AA-BWT were prepared using different types of microporous membranes as substrates, which maintained the porous structure of the membranes and had the characteristics of high flux and fast filtration rate. The surface contact angle and pure water flux analysis showed that the introduction of tannin with multi-phenolic hydroxyl groups increased the hydrophilicity and water flux of the M-TANs. The adsorption performance shows that the adsorption capacity of four kinds of M-TANs for UO_2^{2+} is in the order of PA-BWT > PA-AA-BWT > PVDF-BWT > CELL-BWT, and PA-BWT has the largest adsorption capacity of 0.398 mmol g^{-1}. In addition, the adsorption isothermal and kinetic data of PA-BWT were well fitted by the Langmuir equation and the Elovich model, respectively. The negative values of ΔG for UO_2^{2+} adsorption on PA-BWT indicated that adsorption is a spontaneous and favorable process. These facts indicate that PA-BWT can be used as a low-cost adsorbent for effective removal of UO_2^{2+} from aqueous solutions.

Keywords: plant tannins; microporous membranes; immobilized tannins; membrane adsorption

Citation: Luo, W.; Lin, H.; Wu, Z.; Chen, J.; Chi, R.; Ye, X.; Chen, J. Preparation and Physicochemical Properties of Tannin-Immobilized Membrane Adsorbent. *Appl. Sci.* **2021**, *11*, 9684. https://doi.org/10.3390/app11209684

Academic Editor: Stefano Salvestrini

Received: 1 September 2021
Accepted: 13 October 2021
Published: 17 October 2021

1. Introduction

Tannin is a class of polyphenol compounds with abundant phenolic hydroxyl groups, and is one of the compounds with the strongest ability to complex with metal ions in natural products [1–5]. However, plant tannins are easily soluble in water, and generally cannot be directly used for the treatment of heavy metal ions in wastewater. They need to be immobilized on a water-insoluble carrier to obtain immobilized tannin adsorption materials. In order to overcome this shortcoming, researchers have tried to immobilize tannins on various water-insoluble substrates and use them through fixed bed adsorption [6–10]. However, the fixed bed method has some disadvantages in removing large amounts of wastewater, such as long diffusion distances in porous adsorbents, which leads to low adsorption efficiency. In addition, the accumulation of adsorbent will also cause a loss of adsorption points and higher bed pressure drop. Membrane adsorption is a forced convective mass transfer control process, which can significantly shorten the diffusion distance and overcome the pressure drop problem of traditional fixed bed adsorption [11–14]. The adsorption rate is mainly controlled by the binding kinetics of the adsorbate and membrane adsorption sites. A higher feed rate can be achieved under the premise of using the adsorption site to achieve high-speed adsorption [15,16]. Inspired by the performance of tannins to form stable complexes with metal ions and the low pressure drop and high flux characteristics of microporous membranes, we have combined tannins with membranes to develop a new type of tannin-immobilized membrane adsorption material. The choice

of a microporous membrane and the immobilization method is the key to the preparation of immobilized tannin membrane materials. Commonly used organic microporous membranes include polyamide, polytetrafluoroethylene, polyvinylidene fluoride, and cellulose membranes.

As a commonly used filter membrane, polyamide (PA) microporous membranes have good hydrophilicity, can withstand acid and alkali solutions of appropriate concentrations, and have functional groups such as -NH, -NH_2, and -C=O in their molecular structure [17,18]. Studies have shown that the amino group itself can interact with tannins through hydrogen bonds, and tannins can also react with -NH and -NH_2 through aldehyde cross-linking [19]. Therefore, tannin can be immobilized on the PA membrane by the adsorption cross-linking method. In addition, according to the reaction characteristics of tannins, the hydroxyl groups in tannins can undergo an esterification reaction with carboxyl groups [20]. Therefore, PA membrane can also be grafted onto carboxyl compounds and tannins can then be immobilized through the esterification reaction. Polyvinylidene fluoride (PVDF) microporous membranes are also a common commercial filter membrane [21]. They have the advantages of high mechanical strength and wide pH resistance, but they are hydrophobic membranes, which usually need to be hydrophilically modified before they can be used in wastewater treatment. Light-initiated grafting, especially ultraviolet light-initiated grafting, is a technique that forms free radical active centers on the surface of polymers and initiates graft polymerization modification on the surface of polymers [22]. It is a widely used surface modification technique which is also commonly used in the modification of PVDF membranes. In view of this, UV radiation was used to conduct light-initiate grafting on the surface of the PVDF membrane to immobilize the tannin. It has been reported in the literature that dopamine is rich in catechins groups and can stably adhere to a variety of media through covalent and non-covalent interactions and its key functional group is catechol [23,24], while tannin is a plant polyphenol that is rich in catechins and pyrogallol functional groups. Studies have found that in the presence of oxygen, tannins can be coated on various organic and inorganic substrates in a buffer solution (pH 7~8) [25], which is similar to dopamine polymer coatings. Based on the characteristics of tannins, tannins can be immobilized on the cellulose membrane (CELL) by dip coating.

Herein, we selected typical polyamide microporous membranes, polyvinylidene fluoride microporous membranes, and cellulose microporous membranes as basic materials, with black wattle tannin as a typical representative, to prepare tannin-immobilized membranes (M-TANs). A series of physical and chemical properties such as the grafting degree of tannin and the pore size, water flux, and hydrophilicity of the tannin-immobilized microporous membrane were studied. Through the above research, the preparation method of tannin-immobilized microporous membrane adsorbents was established.

2. Materials and Methods

2.1. Materials

The polyamide microporous membrane (PA: the surface porosity is 70%, the average pore size was 0.45 μm, the membrane thickness was 150 μm, and the membrane diameter was 50 mm) and cellulose microporous filter membrane (CELL: the surface porosity was 70%, the average pore size was 0.45 μm, the thickness was 140 μm, and the diameter was 50 mm) were provided by Shanghai Xinya Filtration Instrument Co., Ltd. The polyvinylidene fluoride microporous membrane (PVDF: the surface porosity was 70%, the average pore size was 0.45 μm, the membrane thickness was 190 μm and the the membrane diameter was 50 mm) was purchased from Laisheng Filter Equipment Factory. Black wattle tannin was obtained from Dymatic Chemicals, Inc (China). Uranyl nitrate hexahydrate ($UO_2(NO_3)\cdot 6H_2O$) was produced by Hubei Chushengwei Chemical Co., Ltd. NaCl, $NaHCO_3$, $MgCl_2$, $CaCl_2$, $CuSO_4$, NaCl, and glutaraldehyde (50%) were all analytically pure, and were purchased from Chengdu Kelon Chemical Reagent Factory, China. Glycidyl methacrylate (GMA) was obtained from Shanghai Aladdin Biochemical Technology Co.,

Ltd. Reagents such as benzophenone were of analytical grade, and were provided by Chengdu Kelon Chemical Reagent Factory, China.

2.2. Preparation of Microporous Membrane Immobilized Tannin

The preparation procedures of PA-BWT mainly contained two steps: adsorption and covalent cross-linking (Schematic S1). The polyamide microporous membrane was soaked in 0.5 wt% black wattle tannin aqueous solution for 15 h to obtain the adsorption equilibrium, and then the surface was washed with deionized water to remove extra tannin. The membrane was placed in a 10 wt% glutaraldehyde solution, was covalently cross-linked at 303 K for 3 h, and was then thoroughly washed with deionized water and ethanol to remove the residual cross-linking agent and uncross-linked tannin on the surface. Thus, the PA-BWT was obtained.

The PA membrane was immersed in 100 mL of cerium ammonium nitrate solution, initiated at 40 °C for 0.5 h. Then acrylic acid (AA) was added to react with the PA membrane at 40 °C for 3 h, and the membrane was washed with deionized water. The grafted PA-AA was obtained, and then it was placed in a 1 wt% tannin solution and reacted at 30 °C for 5 h so that the hydroxyl groups in the tannins could be esterified with the carboxyl groups. Finally, after washing with deionized water, the PA-AA-BWT was obtained (Schematic S2).

The PVDF membrane was soaked in a 5 wt% benzophenone (BP) solution for 20 min to allow for full adsorption of the BP onto the membrane. After which, the BP was activated under a 160 W UV lamp for 30 min. The activated PVDF membrane was immersed in a 5 wt% glycidyl methacrylate (GMA) solution and irradiated under a 160 W UV lamp for 1 h to initiate a photo-initiated grafting. Next, the PVDF membrane grafted with GMA was added to a 1 wt% black wattle bark tannin solution to react for a certain time, so that the tannins were chelated onto the PVDF membrane. Finally, deionized water and ethanol were used to remove the residual crosslinking agent and extra tannins on the surface to obtain PVDF-BWT (Schematic S3).

Utilizing the reactive characteristics of tannin which are similar to those of dopamine, the tannin could be immobilized on the CELL membrane by dip coating. A 1 wt% alkaline tannin solution was prepared with Tris-buffer (100 mL, pH = 7.8, 50 mM), and the pretreated CELL membrane was immersed in the alkaline tannin solution for a certain time. During this process, tannin oxidation initiated an aggregation and deposited on the surface of the film to tune its wettability. Finally, after washing with deionized water, the CELL-BWT was obtained (Schematic S4).

2.3. Material Characterization

The grafting degree of tannin was determined by a weighing method. Before weighing, the samples were dried in an oven at 80 °C for 2 h, and the tannin grafting degree was calculated as follows: tannin grafting degree = $(W_1\text{-}W_0)/W_1$, where W_0 is the mass of the film before immobilizing tannin (mg); W_1 is the mass (mg) of M-TAN after immobilizing the tannin; and the grafting degree is expressed in mg (tannin)/g (film). The surface morphology of the membranes was observed using a scanning electron microscope (FESEM, JSM-7500F, JEOL, Japan) at an accelerating voltage of 3 kV; the samples were adhered on a holder using a conductive carbon tape before investigation. An X-ray photoelectron energy spectrum analyzer (XPS, Thermo Scientific Escalab 250XI, USA) was used to analyze the chemical composition of the material surface; these samples were loaded on a sample holder for the study without any further treatment. The static water contact angle (contact angle measuring instrument, Krüss, DSA30, Germany) was used to characterize the static wettability of the material surface.

2.4. Water Flux Measurement

The experiment used a membrane filter as the test device, a constant volume of water column as the driving force, and deionized water as the test water. The constant flow pump was adjusted to ensure a constant height of the water column. The water output Q

of the membrane filter per unit time was recorded, and the effective filtration area A of the membrane was calculated. The pure water flux Jw of the microporous membrane under this pressure was calculated according to the following formula: Jw = Q/A, where Jw is the pure water flux (L m^{-2} h^{-1}), Q is the flow of water (L), and A is the membrane area (m^2).

2.5. Adsorption Isotherm

Adsorption isotherm studies were carried out in 50 mL solutions with an initial UO_2^{2+} concentration ranging from 0.1 to 2 mmol/L. The pH of the solutions was adjusted to 5.0, 0.180 g of PA-BWT was suspended in the solutions, and then the adsorption experiments were conducted with constant stirring for 24 h at 303, 313, 323, and 333 K, respectively. The concentration of UO_2^{2+} after the adsorption equilibrium was attained was analyzed by ICP-AES, and adsorption capacity was calculated according to Equation (1):

$$q_e = \frac{V(C_0 - C_e)}{m} \quad (1)$$

where C_0 and C_e represent the initial and the equilibrium UO_2^{2+} concentration (mg·L^{-1}), respectively; V is the volume of the UO_2^{2+} solution (L); and m is the dosage of the absorbent (g).

2.6. Adsorption Kinetics

The adsorption procedure was similar to that of the adsorption isotherm study, but the concentration of UO_2^{2+} was analyzed at a regular interval by ICP-AES during the adsorption process. The adsorption capacity at time t (min) was obtained by a mass balance calculation and was denoted as q_t (mg/g).

3. Results and Discussion

The tannin grafting degrees of the four kinds of M-TANs are shown in Figure 1. The tannin grafting degrees of the all M-TANs are relatively large, reaching more than 180 mg g^{-1}. However, the tannin grafting degrees of M-TANs prepared by different methods were diverse. Among them, PA-BWT had the maximum grafting degree of 215 mg g^{-1}, followed by PA-AA-BWT and PVDF-BWT. CELL-BWT had the smallest grafting degree. This may be because the PA membrane contains many amino groups, which can interact with tannins through hydrogen bonding so that more tannins can be adsorbed on the membrane. Then, through the cross-linking of glutaraldehyde, the tannin is covalently cross-linked and immobilized on the membrane. Compared with PA-BWT, the tannin grafting degree of PA-AA-BWT was not high. This is because the grafting rate of methacrylic acid is lower, so there is less tannin immobilized by the esterification reaction. For PVDF-BWT, benzophenone is used as the initiator in the light-initiated grafting process, and its molecular structure has two benzene rings, resulting in a large steric hindrance and low grafting degree. When CELL-BWT is prepared by the dipping method, tannin is fixed to the membrane through non-covalent bonding. The tannin on the M-TAN prepared by this method can easily fall off, so the grafting degree of CELL-BWT was the lowest.

Figure 2 shows the scanning electron micrographs (FESEM) of the four membranes before and after immobilizing the tannins. As shown in Figure 2, no matter what kind of membrane or method was used to prepare the M-TANs, the membrane structure of the raw material was still maintained, while the membrane pore size and pore wall roughness changed. Compared with the original PA (Figure 2a), the pore size of PA-BWT (Figure 2b) was significantly reduced to 0.5 ~ 0.2 μm. Similar to PA-BWT, the FESEM images of PA-AA-BWT show similar changes (Figure 2c,d). Figure 2e,f shows FESEM images of PVDF and PVDF-BWT. There were many micropores on the surface of the PVDF membrane with a wide pore size distribution ranging from 5.0 to 1.0 μm, and the membrane pore walls were relatively smooth. Figure 2f shows the structure of the PVDF-BWT membrane; it can be seen that the pore size of the membrane was reduced due to the adhesion of tannin. The membrane pore wall of PVDF-BWT became rougher. Figure 2g,h shows FESEM images of

CELL and CELL-BWT. Compared with the other three M-TANs, the structural changes of CELL-BWT before and after the immobilization of tannins were not obvious. The original CELL structure (Figure 2g) was densely packed with cotton fiber bundles, and the fiber surface was relatively smooth. Compared with CELL, the surface of CELL-BWT fiber became rough, but the pore structure did not change much (Figure 2h). This is because the tannin grafting degree of CELL-BWT prepared by the dip coating method was not large, and the effect on the pore size was not obvious.

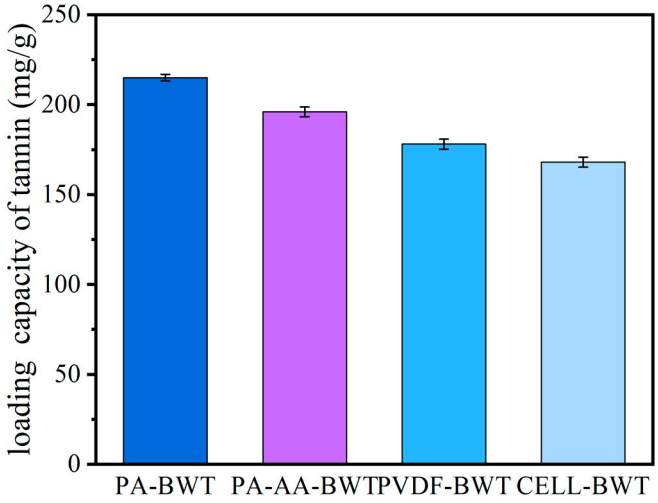

Figure 1. The tannin loading capacity of the tannin-immobilized membranes: PA-BWT, PA-AA-BWT, PVDF-BWT, and CELL-BWT.

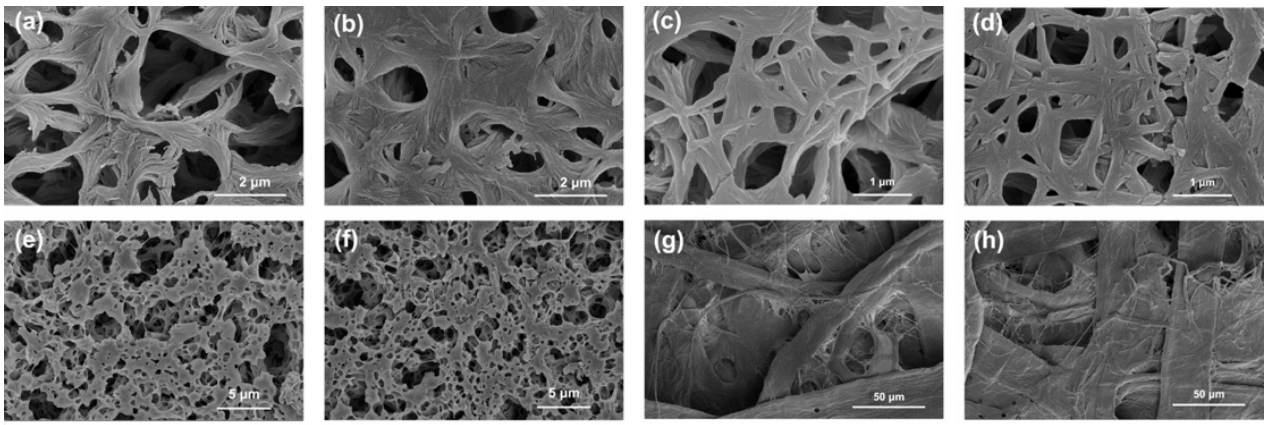

Figure 2. FESEM images of (**a**,**b**) PA and PA-BWT, (**c**,**d**) PA-AA and PA-AA-BWT, (**e**,**f**) PVDF and PVDF-BWT, and (**g**,**h**) CELL and CELL-BWT.

Figure 3a–d shows the XPS full spectrum and O 1s spectrum of PA and PA-BWT. The characteristic peaks of C 1s, N 1s, and O 1s appeared in the spectra of PA and PA-BWT, but after the tannin was immobilized, the peak intensity of C 1s and O 1s in PA-BWT was much higher than that of N 1s. This is because tannins are mainly C, H, and O elements, so when tannins are immobilized on the PA membrane, the relative content of N 1s decreases. In addition, as shown in Figure 3b, the O 1s in PA is mainly a C=O characteristic peak with a binding energy of 531.2 eV. However, except for the above C=O peak of O 1s of PA-BWT, the immobilization of tannin also introduced an additional C–O peak with a binding energy of 532.9 eV, indicating that PA-BWT was successfully prepared. The full XPS spectra of PVDF and PVDF-BWT and the partial spectra of O1s are shown in Figure 3e,f. The characteristic peaks of C 1s and F 1s at binding energies of 285.08 eV and 684.8 eV appeared in both PVDF

and PVDF-BWT. However, the difference is that the characteristic peak of O 1s at a binding energy of 531.1 eV newly appeared in PVDF-BWT, and the peak intensity of F 1s decreased, while the peak intensity of C 1s increased. This is due to the introduction of tannins containing multiple benzene rings and phenolic hydroxyl groups, thereby introducing the O element and increasing the C 1s content on the surface of PVDF-BWT. Further analysis of the O 1s spectrum (as shown in Figure 3g,h) indicates that the intensity of the O 1s peak in the PVDF spectrum was extremely low, which may have been caused by impurities on the surface of the PVDF membrane. In contrast, the O 1s peak intensity of PVDF-BWT was greatly improved, and could be divided into two peaks, C=O and C–O, with binding energies of 531.6 eV and 532.5 eV, respectively, which were caused by the immobilizing of tannins. The XPS spectrum of PA-AA-BWT were similar to those of PA-BWT (Figure 3i,j). The N 1s peak intensity of PA-AA-BWT was reduced after the tannin was immobilized by the esterification reaction. Compared with PA-BWT, the content of C 1s and O 1s in PA-AA-BWT changed. The content of O 1s in PA-AA-BWT increased and was higher than that of C 1s due to the introduction of the carboxyl group in the esterification reaction of methacrylate. Figure 3k,l shows the XPS spectra of CELL and its tannin-immobilized membrane CELL-BWT. Both CELL and CELL-BWT contain C and O elements. However, in Figure 3l, after immobilizing tannin, the peak intensity of O 1s decreased and the peak intensity of C 1s increased. This is due to the introduction of tannins with multiple benzene rings, thereby increasing the C 1s content on the surface of CELL-BWT. The FTIR spectra also confirmed the successful synthesis of four M-Tans (Figure S1).

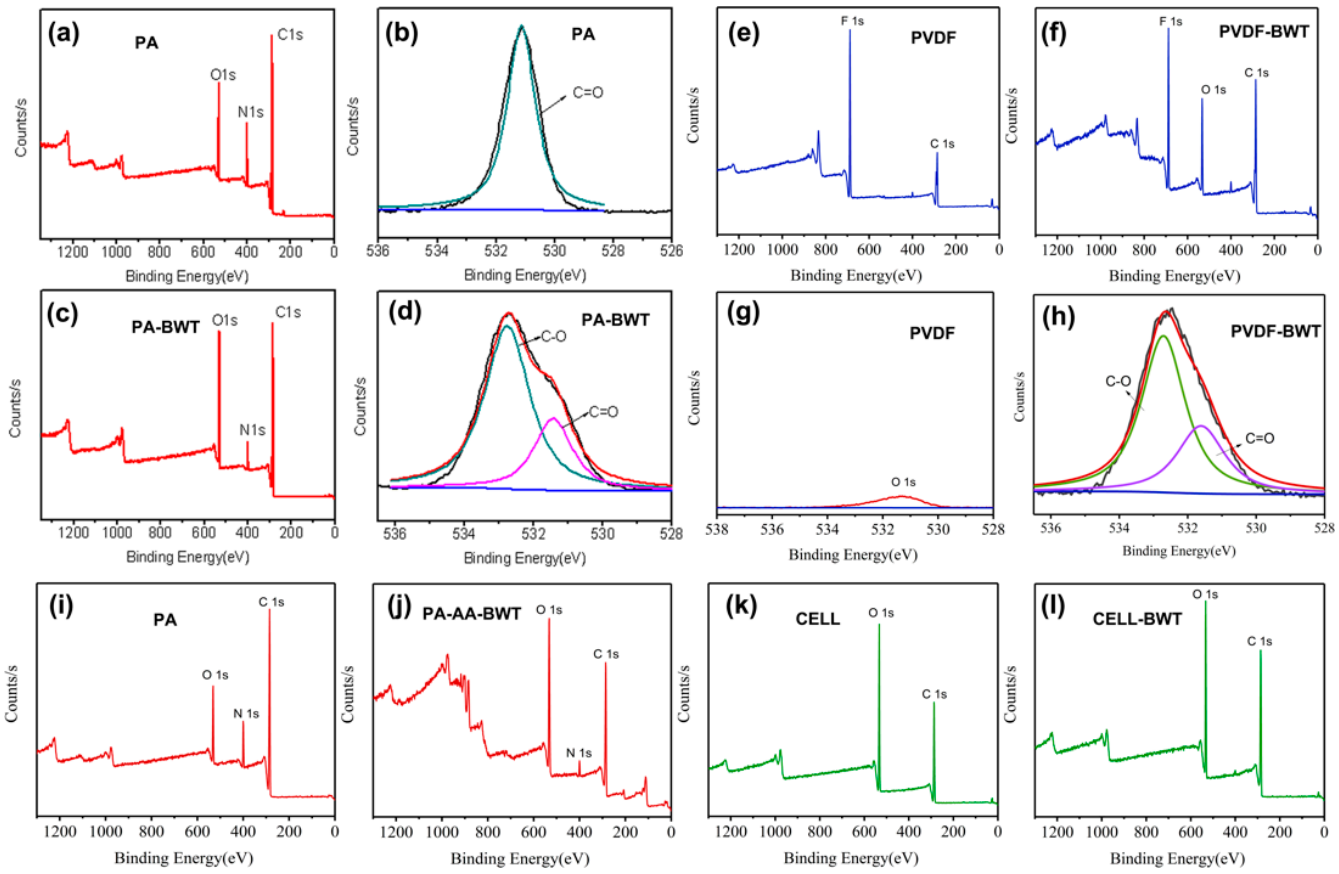

Figure 3. High resolution XPS spectra and O 1s spectra of (**a**–**d**) PA and PA-BWT, (**e**–**h**) PVDF and PVDF-BWT, (**i**,**j**) PA and PA-AA-BWT, and (**k**,**l**) CELL and CELL-BWT.

The hydrophilicity of the microporous membrane and the M-TANs were evaluated by testing the water contact angle of the surface. Figure 4a shows the water contact angles of various membranes and M-TANs. As shown in Figure 4a, the hydrophilicity of the PA was significantly enhanced after immobilizing the tannin, and the water contact angle was reduced from the original 88.5° to 70.1°. This is because after the cross-linking reaction between the 6,8 positions on the tannin A ring and the amino group of the PA, the unreacted phenolic hydroxyl group on the tannin is exposed to the surface of the M-TANs, and the phenolic hydroxyl group is a strong hydrophilic group [26]. Therefore, the hydrophilicity of PA-BWT was enhanced. The hydrophilicity of PA-AA-BWT was also enhanced, and the water contact angle was reduced from the original 88.5° to 72.5°. However, compared with PA-BWT, the hydrophilicity of PA-AA-BWT was not as strong due to a smaller tannin grafting degree. PVDF membrane is a hydrophobic microporous membrane with a water contact angle of 110.4°, but the hydrophobicity of PVDF-BWT immobilized with tannin obviously changed greatly, and the water contact angle directly dropped to 85.2°. It changed from a hydrophobic membrane to a hydrophilic membrane, which is also caused by the tannins rich in hydrophilic phenolic hydroxyl groups. The CELL membrane itself is a hydrophilic membrane with a water contact angle of 81.2°. After the tannin was immobilized by the dip coating method, the hydrophilicity of CELL-BWT was slightly reduced, and the contact angle increased to 84.2°. This is because when the tannin is immobilized by the dip coating method, the pH value of the solution is adjusted to alkaline. At this time, the phenolic hydroxyl groups on tannins are oxidized to quinones [27], and the tannins containing hydrophobic benzene rings are mainly hydrophobic due to the loss of phenolic hydroxyl groups, so the hydrophilicity of CELL-BWT was reduced. The pure water fluxes of the four organic filter membranes and their cured tannin membranes are shown in Figure 4b. After immobilizing the tannins, the pure water fluxes of both PA and PVDF membranes increased. The pure water flux of the PA membrane was 70.25 L m^{-2} h^{-1}, while the pure water flux of PA-BWT and PA-AA-BWT after the tannin was immobilized increased to 110.52 and 108.45 L m^{-2} h^{-1}, respectively. Although immobilized tannin reduces the pore size of the membrane and may slightly reduce the flux of pure water, the rich phenolic hydroxyl groups on the tannin greatly increase the hydrophilicity of the membrane, which is beneficial for the flux of pure water. The pure water flux of PA-BWT was greater than that of PA-AA-BWT due to the former's larger tannin grafting degree. The pure water flux of the hydrophobic PVDF membrane is basically 0 without external pressure, while the pure water flux of PVDF-BWT can reach 54.65 L m^{-2} h^{-1} without external pressure. Such a significant change is also caused by the immobilization of tannins. This shows that the immobilization of tannin on the membrane not only enables the membrane to have adsorption properties but can even change the hydrophilicity and hydrophobicity of the membrane, expanding the application of tannin in membrane surface modification. The flux of pure water of CELL and CELL-BWT did not change much before and after tannin immobilization, and the flux of pure water of CELL-BWT even decreased slightly due to its slight reduction of hydrophilicity and pore size.

In order to investigate the adsorption performance of different M-TANs, UO_2^{2+} was used as the adsorption object to determine the adsorption capacity of these four M-TANs. The adsorption capacities of the four M-TANs for UO_2^{2+} are shown in Figure S2. The adsorption capacities of PA-BWT, PA-AA-BWT, PVDF-BWT, and CELL-BWT for UO_2^{2+} are 0.209, 0.197, 0.186, and 0.102 mmol g^{-1}, respectively. It can be seen that, except for CELL-BWT, the adsorption capacities of other M-TANs for UO_2^{2+} are relatively large, and the PA-BWT > PA-AA-BWT > PVDF-BWT > CELL-BWT is arranged according to the adsorption capacity, which is in direct proportion to the grafting degree of tannin. It is known that the original PA, PVDF, and CELL membranes have no adsorption capacity for UO_2^{2+}, indicating that the adsorption of UO_2^{2+} by the M-TANs is mainly dependent on the tannins. Therefore, the adsorption capacity for UO_2^{2+} increased with the increase of tannin grafting degree.

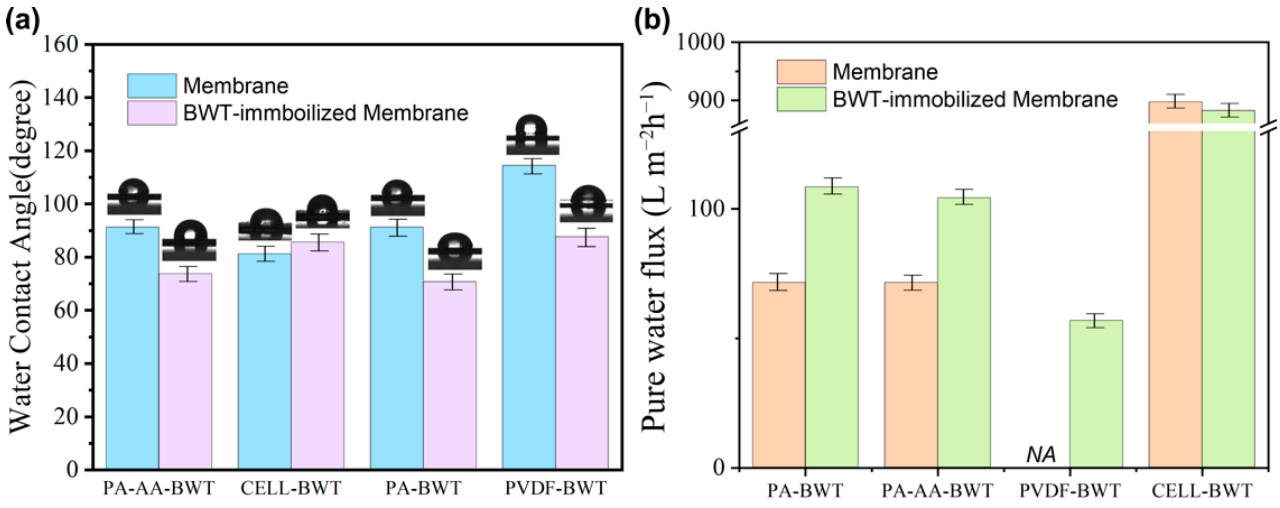

Figure 4. (**a**)Water contact angle of membrane and BWT-immobilized membrane and (**b**) pure water flux of membrane and BWT-immobilized membrane.

The adsorption performance of UO_2^{2+} by PA-BWT was further studied. PA-BWT shows a considerable adsorption capacity to UO_2^{2+}, reaching 0.398 mmol g^{-1} at 333 K with an initial UO_2^{2+} concentration of 2 mmol L^{-1}, as shown in Figure 5a. In addition, the adsorption capacity was increased with the increase of temperature, suggesting that the process of UO_2^{2+} adsorption of PA-BWT is endothermic in nature. To clearly understand the adsorption process, adsorption isotherm data were further analyzed by the Langmuir models (Figure 5b) [28,29]:

$$\text{Langmuir equation}: \frac{C_e}{q_e} = \frac{1}{b \cdot q_{\max}} + \frac{C_e}{q_{\max}} \quad (2)$$

$$\text{Freundlich equation}: \ln q_e = \ln K + \frac{1}{n} \ln C_e \quad (3)$$

where q_e (mmol/g) is the equilibrium adsorption capacity; $q_{\max}$ (mmol/g) is the maximum adsorption capacity; C_e (mmol/L) is the equilibrium concentration; and b (L/mg) is the coefficient related to the affinity of the binding sites ($b = k_a/k_d$, k_a is the rate constant of adsorption, k_d is the rate constant of desorption). K and $1/n$ are the constants that are related to the adsorption capacity and the adsorption intensity, respectively.

As summarized in Table 1, the Langmuir model provides a much better description of the isotherm data with a correlation constant higher than 0.99, and the calculated theoretical adsorption capacity is close to those obtained from the experiments. Consequently, the Langmuir model is more suitable for the description of adsorption isotherms of UO_2^{2+} on PA-BWT. Considering that the adsorption capacity was increased with the increase of temperature, it is reasonable to conclude that UO_2^{2+} is chemically adsorbed with monolayer coverage on the surface of PA-BWT.

As shown in Figure 5c, it can be observed that the adsorption rate of PA-BWT is quite rapid, and adsorption equilibrium is attained at about 200 min. At higher temperatures, the time to attain adsorption equilibrium is also reduced. In order to understand the adsorption process of PA-BWT to UO_2^{2+}, adsorption kinetic data were fitted by the Lagergren models (Figure 5d) [30–32]:

Lagergren pseudo-first-order kinetic model:

$$\ln(q_e - q_t) = \ln q_e - k_1 t \quad (4)$$

Lagergren pseudo-second-order kinetic model:

$$\frac{t}{q_t} = \frac{1}{k_2 q_e^2} + \frac{t}{q_e} \quad (5)$$

where q_e and q_t (mmol/g) are the adsorption capacity of UO_2^{2+} at equilibrium and at time t, respectively; k_1 (min^{-1}) is the first-order rate constant, and k_2 (g/(mmol·min)) is the second-order rate constant.

As listed in Table 2, the correlation coefficients obtained by the pseudo-second-order kinetic model fitting are very close to 1.0 compared to those of the pseudo-first-order model, suggesting that the chelating interaction between UO_2^{2+} and PA-BWT is the rate-control step of the adsorption process.

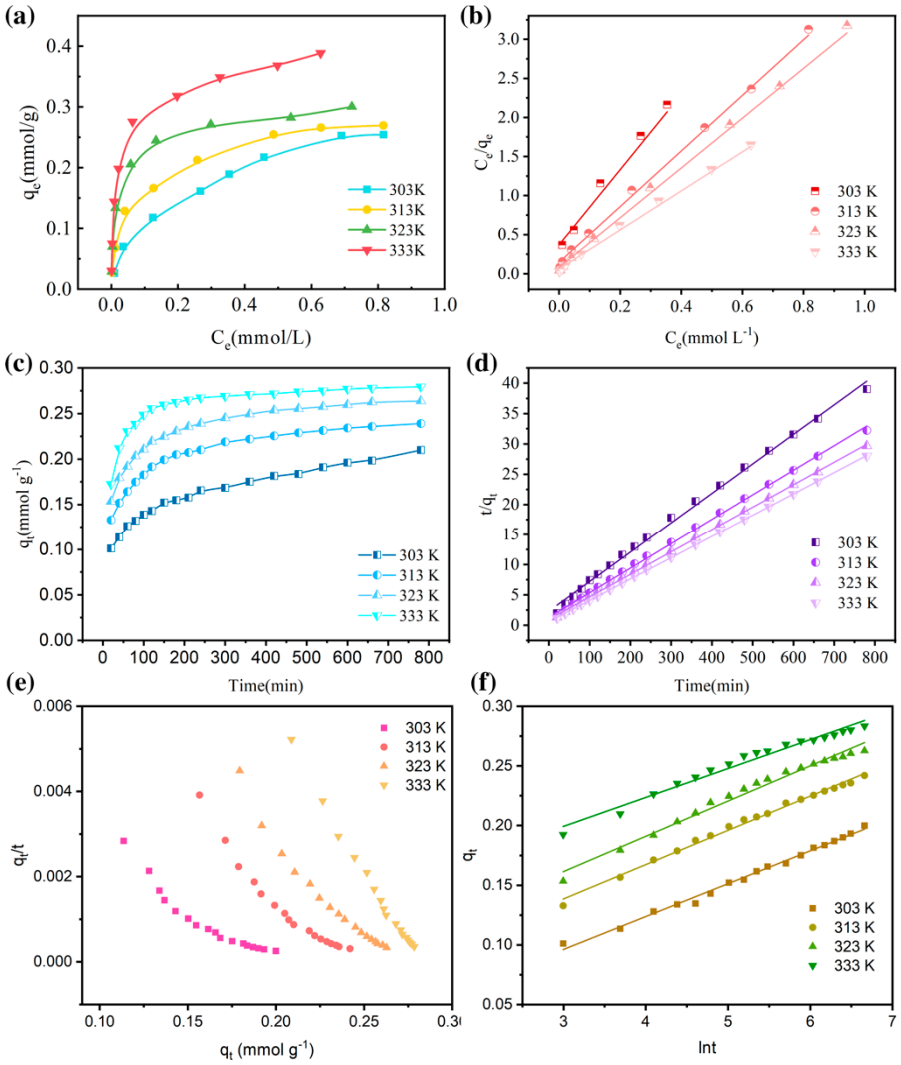

Figure 5. Adsorption isotherms of PA-BWT to UO_2^{2+}: UO_2^{2+} ion concentration 0.1–2 mmol/L, pH 5.0: (**a**) adsorption isotherms and (**b**) regression by the Langmuir equation. Adsorption kinetics of UO_2^{2+} on PA-BWT: UO_2^{2+} concentration 1 mmol/L, pH 5.0: (**c**) adsorption kinetics and (**d**) regression by the pseudo-second-order equation. (**e**) Regression by the pseudo-second-order model (PSO) expressed in a different linearized form. (**f**) Regression by the Elovich model.

Table 1. Langmuir and Freundlich parameters of UO_2^{2+} adsorbed on PA-BWT.

Temperature (K)	Langmuir				Freundlich		
	q_{max} (mmol/g)	B (L/mmol)	$q_{max,exp}$ (mmol/g)	R^2	K	1/n	R^2
303	0.209	12.982	0.192	0.9825	6.72	0.5132	0.9665
313	0.282	24.201	0.269	0.9992	14.53	0.4610	0.9635
323	0.314	40.043	0.317	0.9975	23.21	0.4662	0.9256
333	0.401	41.565	0.405	0.9933	28.34	0.4956	0.9434

$q_{max,exp}$: the maximum adsorption capacity determined by experiments.

Table 2. Fitting parameters of the pseudo-first-order and pseudo-second-order models.

Temperature (K)	Pseudo-Second-Order				Pseudo-First-Order	
	R^2	k_2	$q_{e.cal}$ (mmol/g)	$q_{e,exp}$ (mmol/g)	R^2	k_1
303	0.9975	0.101	0.206	0.201	0.7708	0.553
313	0.9978	0.123	0.246	0.240	0.7899	0.566
323	0.9998	0.142	0.269	0.262	0.8789	0.664
333	0.9998	0.223	0.284	0.279	0.9701	0.605

$q_{e,exp}$: the maximum adsorption capacity determined by experiments. $q_{e.cal}$: the maximum adsorption capacity determined by calculation.

In order to further explore the adsorption kinetics of UO_2^{2+} on PA-BWT, we also used the pseudo-second-order model (PSO) expressed in a different linearized form ($q_t/t = k_2 q_e^2 - k_2 q_e q_t$.) for fitting analysis [33]. As shown in Figure 5e, the data are not distributed along a straight line, so it follows that the PSO is not suitable for describing the adsorption kinetics. In addition, the results of fitting using the Elovich model ($q_t = 1/\beta * \ln(1 + \alpha\beta t)$, where q_t (mmol/g) is the adsorption capacity of UO_2^{2+} at time t, α is the initial adsorption rate constant, and β is the chemical adsorption activation energy parameters) are shown in Figure 5f, and the correlation coefficient $R^2 > 0.99$ obtained by fitting indicates that the Elovich model is more appropriate to describe the adsorption of UO_2^{2+} on PA-BWT, which is a chemical adsorption process. The Weber–Morris model was also used for fitting. As shown in Figure S3, the adsorption process is divided into two stages, namely the surface diffusion process and the intraparticle diffusion process. The straight line through the origin indicates that surface diffusion and intra-particle diffusion jointly control the adsorption process of PA-BWT on UO_2^{2+}.

The thermodynamic behaviors of UO_2^{2+} ion adsorption onto PA-BWT were evaluated by employing the following equations [15]:

$$\ln bx = \ln\ b\prime - \Delta H^\circ/RT \quad (6)$$

$$\ln\left(\frac{1}{b}\right) = \Delta G^\circ/RT \quad (7)$$

$$\Delta S^\circ = (\Delta H^\circ - \Delta G^\circ)/T \quad (8)$$

where R (8.314 J/K mol) is the ideal gas constant; T (K) is the temperature; Kd (L/g) is the distribution coefficient; C_0 (mg/L) is the initial concentration; ΔH°, ΔS°, and ΔG° (kJ/mol) are the enthalpy change, the entropy change, and the Gibbs free energy change in a given process, respectively; b is the Langmuir parameter, whereas b′ is a constant; and x(g/mol) is the adsorbent molecular weight. Thermodynamic parameters were calculated according to Equations (6)–(8) and illustrated in Table 3. ΔG° values are negative for UO_2^{2+} adsorption onto the PA-BWT surface, indicating that adsorption is a spontaneous process in standard conditions [34]. The positive value of ΔS° suggests the affinity of PA-Tan toward UO_2^{2+} ions. The positive value of ΔH° confirms the endothermic nature of the adsorption process.

Table 3. Langmuir parameters and thermodynamic parameters.

Temperature (K)	Thermodynamic Parameter		
	ΔG° **(kJ/mol)**	**ΔS°** **(kJ/(mol K))**	**ΔH°** **(kJ/mol)**
303	−9.20	0.163	40.28
313	−7.33	0.152	
323	−6.08	0.143	
333	−6.23	0.139	

The stability experiment of M-TANs was carried out by immersion oscillation experiment under different temperatures and pH values. As shown in Figure S4a,b, the M-TANs were immersed in pure water at 20 °C and 50 °C and shaken for a week to examine their stability at different temperatures. PA-BWT, PVDF-BWT, and PA-AA-BWT did not change significantly, while the color of CELL-BWT was slightly lighter. This indicates that the PA-BWT, PVDF-BWT, and PA-AA-BWT prepared by the covalent cross-linking method have a high stability, and the tannins will not fall off even under long-term oscillating soaking, while the tannins in CELL-BWT, combined by hydrogen bonding, can easily fall off the membrane under long-term shaking and soaking. The results of further measuring their water flux are shown in Figure 6a. The water flux of PA-BWT, PVDF-BWT, and PA-AA-BWT did not change significantly, but the water flux of CELL-BWT increased slightly. This is because the shedding of tannins on the membrane increases the hydrophilicity and pore size of CELL, thereby increasing the water flux. Corresponding to the degree of tannin grafting, the adsorption capacity of PA-BWT, PVDF-BWT, and PA-AA-BWT remained basically unchanged, while the adsorption capacity of CELL-BWT decreased significantly (Figure 6b), which was attributed to the shedding of tannin. The M-TANs were immersed in pure water with pH = 2 and pH = 9 at room temperature and shaken for a week to investigate their stability at different pH values. As shown in Figure S4c,d, the morphology of the M-TANs after oscillating immersion in different pH solutions did not change, and there was no damage or corrosion phenomenon, indicating that they could still maintain their original structure under alkaline/acidic conditions. Figure 6c,d shows the pure water flux and adsorption capacity of UO_2^{2+} of M-TANs before and after oscillating immersion in different pH solutions. PA-BWT, PVDF-BWT, and PA-AA-BWT had no change in water flux and UO_2^{2+}adsorption capacity after being immersed in different pH solutions for a long time, which indicates that they have good stability and anti-pollution performance. However, for Cell-BWT, the adsorption capacity of UO_2^{2+} decreased greatly after a long period of oscillating soaking, indicating that the tannin on the surface of CELL-BWT fell off seriously. This indicates that M-TANs prepared by the covalent cross-linking method have better stability and firm tannin immobilization.

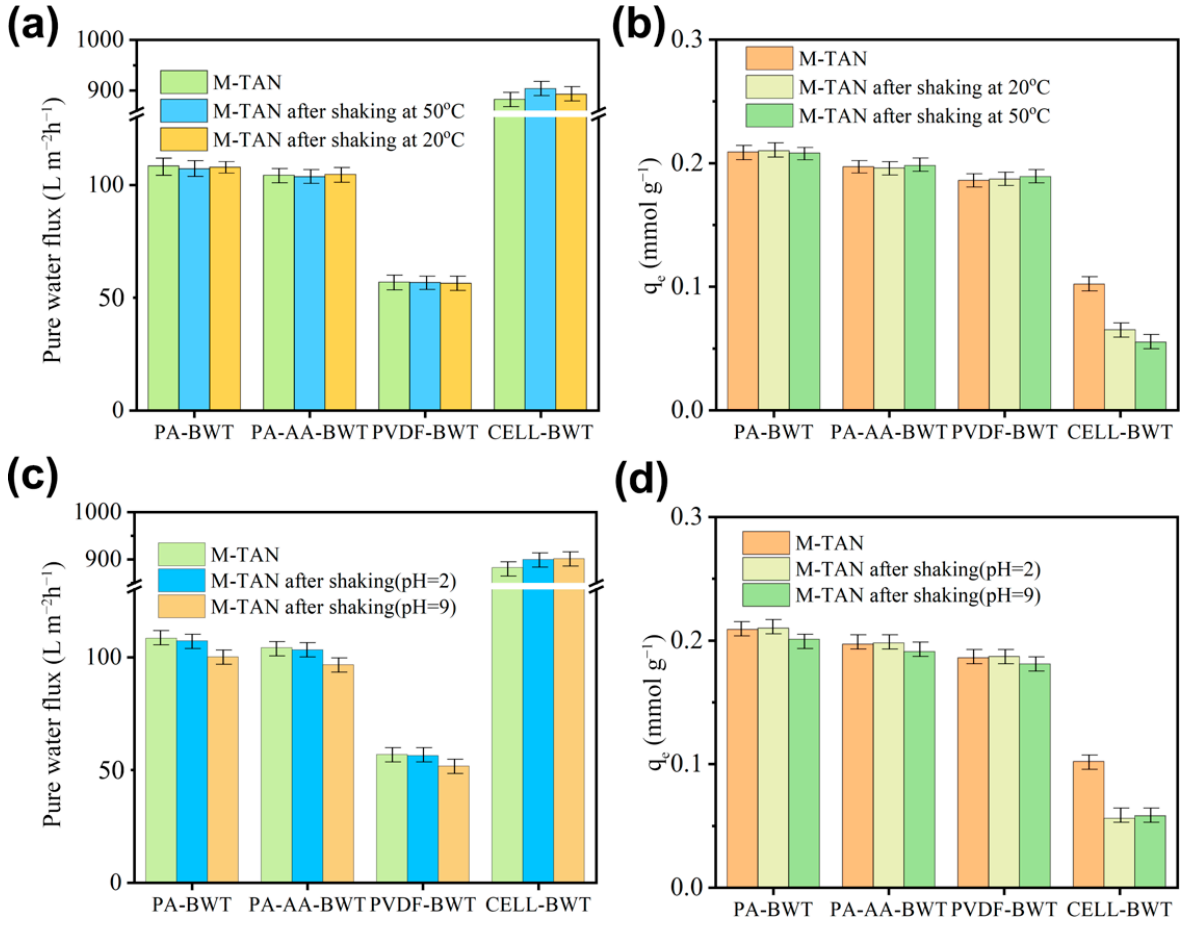

Figure 6. Water flux and adsorption capacity of different M-TANs before and after long-term shaking and soaking at (**a**,**b**) different temperatures and (**c**,**d**) pH.

4. Conclusions

Typical polyamide, polyvinylidene fluoride, and cellulose microporous filter membranes were selected as basic materials using different immobilizing methods to prepare tannin-immobilized membranes: PA-BWT, PVDF-BWT, CELL-BWT, and PA-AA-BWT. The tannin grafting degrees of M-TANs prepared by different methods are different: the PA-BWT had the maximum grafting degree, followed by PA-AA-BWT and PVDF-BWT, and the minimum grafting degree belonged to CELL-BWT. The contact angle of the surface water proves that the introduction of tannins rich in phenolic hydroxyl groups improved the hydrophilicity of the original membrane, and the higher hydrophilicity resulted in a greater water flux. The adsorption performance studies show that PA-BWT had the largest adsorption capacity for UO_2^{2+}. The PA-BWT exhibited a maximal adsorption capacity (0.4 mmol/g) at pH 5.0 and 333 K with an initial U(VI) concentration of 2 mmol/L. In addition, the adsorption isothermal and kinetic data were well fitted by the Langmuir equation and the Elovich model, respectively. The PA-BWT, PVDF-BWT, and PA-AA-BWT prepared by the covalent cross-linking method had good stability under different environmental conditions; thus, the membrane structure will not be destroyed, and the tannins on the membrane will not easily fall off. Therefore, PA-BWT exhibits a great potential in practical application for U(VI) removal from aqueous solutions as a low-cost, highly effective, and reusable adsorbent.

Supplementary Materials: The following are available online at https://www.mdpi.com/article/10.3390/app11209684/s1. Schematic S1: Schematic illustration showing the preparation of PA-BWT, Schematic S2: Schematic illustration showing the preparation of PA-AA-BWT, Schematic S3:

Schematic illustration showing the preparation of PVDF-BWT, Schematic S4: Schematic illustration showing the preparation of CELL-BWT, Figure S1: The FTIR spectra of (a)PA and PA-BWT, (b) PA and PA-AA-BWT, (c) PVDF and PVDF-BWT, (d) CELL and CELL-BWT, Figure S2: Adsorption capacity of UO_2^{2+} on different M-TANs: the initial concentration of the UO_2^{2+} solution is 1 mmol L^{-1}, the pH is 5.0, and the adsorption time is 24 h, Figure S3: Adsorption kinetics regression by the Weber-Morris model: $q_t = k_{ip}t^{1/2} + C$, where q_t (mmol/g) are the adsorption capacity of UO_2^{2+} at time t, k_{ip} is Internal diffusion rate constant and C is a constant of the surface boundary layer thickness of the adsorbed material, Figure S4: Digital photos of different M-TAN before and after long-term shaking and soaking at different temperatures (a) 20°C, (b) 50°C, and pH (c) pH=2, (d) pH=9.

Author Contributions: Conceptualization, W.L., X.Y. and J.C. (Jie Chen); Data curation, W.L.; Formal analysis, H.L.; Funding acquisition, X.Y.; Investigation, Z.W.; Methodology, W.L. and X.Y.; Project administration, X.Y.; Software, H.L.; Validation, Z.W., J.C. (Jingteng Chen) and R.C.; Visualization, W.L. and X.Y.; Writing—original draft, W.L.; Writing—review & editing, W.L., X.Y. and J.C. (Jie Chen) All authors have read and agreed to the published version of the manuscript.

Funding: This research was financially supported by the National Natural Science Foundation of China (No. 22008035), the Fujian Industry-University-Research Project (No. 2019H6008), the Natural Fujian Science Foundation National (No. 2020J05131), the Science and Technology Project of Fujian Educational Committee (No. JAT190053), the Fuzhou University Testing Fund of precious 23. apparatus (No. 2020T009), and the Research Initiation Funding of Fuzhou University (No. GXRC-19060).

Conflicts of Interest: The funders had no role in the design of the study; in the collection, analyses, or interpretation of data; in the writing of the manuscript; or in the decision to publish the results.

References

1. Costa, J.M.; Bensi, A.; Romani, G.E.B.; Lana, H.C.; Pereira, R.S.; Giraldi, T.R. Metal Recovery using Tannin Resin: An Alternative for the Treatment of Electronic Waste. *Int. J. Environ. Sci. Nat. Resour.* **2019**, *17*, 1–5. [CrossRef]
2. Sun, X.; Huang, X.; Liao, X.-P.; Shi, B. Adsorptive Recovery of UO22+ from Aqueous Solutions Using Collagen–Tannin Resin. *J. Hazard. Mater.* **2010**, *179*, 295–302. [CrossRef] [PubMed]
3. Oladoja, N.; Alliu, Y.; Ofomaja, A.; Unuabonah, E. Synchronous Attenuation of Metal Ions and Colour in Aqua Stream Using Tannin–Alum Synergy. *Desalination* **2011**, *271*, 34–40. [CrossRef]
4. Lee, S.-Y.; Choi, H.-J. Persimmon Leaf Bio-Waste for Adsorptive Removal of Heavy Metals from Aqueous Solution. *J. Environ. Manag.* **2018**, *209*, 382–392. [CrossRef] [PubMed]
5. Crozier, A.; Jaganath, I.B.; Clifford, M.N. Dietary Phenolics: Chemistry, Bioavailability and Effects on Health. *Nat. Prod. Rep.* **2009**, *26*, 1001–1043. [CrossRef]
6. Huang, X.; Liao, X.; Shi, B. Hg (II) Removal from Aqueous Solution by Bayberry Tannin-Immobilized Collagen Fiber. *J. Hazard. Mater.* **2009**, *170*, 1141–1148. [CrossRef]
7. Zeng, Y.; Liao, X.; He, Q.; Shi, B. Recovery of Th (IV) from Aqueous Solution by Reassembled Collagen-Tannin Fiber Adsorbent. *J. Radioanal. Nucl. Chem.* **2009**, *280*, 91–98. [CrossRef]
8. Bacelo, H.A.; Santos, S.C.; Botelho, C. Tannin-Based Biosorbents for Environmental Applications—A review. *Chem. Eng. J.* **2016**, *303*, 575–587. [CrossRef]
9. Wang, R.; Zhang, Z.; Liu, H.Y. Adsorption Disciplinarian of Metal Ions on Collagen Fiber Immobilized Bayberry Tannin. *Adv. Mater. Res.* **2011**, *391–392*, 1031–1035. [CrossRef]
10. Nakajima, A.; Sakaguchi, T. Recovery of Uranium by Tannin Immobilized on Matrices which Have Amino Group. *J. Chem. Technol. Biotechnol.* **2007**, *47*, 31–38. [CrossRef]
11. Li, C.; Meckler, S.; Smith, Z.P.; Bachman, J.E.; Maserati, L.; Long, J.R.; Helms, B.A. Engineered Transport in Microporous Materials and Membranes for Clean Energy Technologies. *Adv. Mater.* **2018**, *30*. [CrossRef]
12. Li, H.-J.; Cao, Y.-M.; Qin, J.-J.; Jie, X.-M.; Wang, T.; Liu, J.-H.; Yuan, Q. Development and Characterization of Anti-Fouling Cellulose Hollow Fiber UF Membranes for Oil–Water Separation. *J. Membr. Sci.* **2006**, *279*, 328–335. [CrossRef]
13. Tan, Z.; Chen, S.; Peng, X.; Zhang, L.; Gao, C. Polyamide Membranes with Nanoscale Turing Structures for Water Purification. *Science* **2018**, *360*, 518–521. [CrossRef] [PubMed]
14. Ying, Y.; Yang, Y.; Ying, W.; Peng, X. Two-Dimensional Materials for Novel Liquid Separation Membranes. *Nanotechnology* **2016**, *27*, 332001. [CrossRef]
15. Tansel, B. Significance of Thermodynamic and Physical Characteristics on Permeation of Ions During Membrane Separation: Hydrated Radius, Hydration Free Energy and Viscous Effects. *Sep. Purif. Technol.* **2012**, *86*, 119–126. [CrossRef]
16. Kumar, P.; Guliants, V.V. Periodic Mesoporous Organic–Inorganic Hybrid Materials: Applications in Membrane Separations and Adsorption. *Microporous Mesoporous Mater.* **2010**, *132*, 1–14. [CrossRef]

17. Feng, S.; Low, Z.-X.; Liu, S.; Zhang, L.; Zhang, X.; Simon, G.P.; Fang, X.-Y.; Wang, H. Microporous Polymer Incorporated Polyamide Membrane for Reverse Osmosis Desalination. *J. Membr. Sci.* **2020**, *610*, 118299. [CrossRef]
18. Chen, Y.; Qin, J.; Tong, T.; Zhou, H.; Cao, X.; Jin, W. Study on the Effect of Crosslinking Temperature on Microporous Polyamide Membrane Structure and Its Nitrogen/Cyclohexane Separation Performance. *Sep. Purif. Technol.* **2020**, *252*, 117401. [CrossRef]
19. Collins, R.A.; Ng, T.B.; Fong, W.P.; Wan, C.C.; Yeung, H.W. Removal of Polyphenolic Compounds from Aqueous Plant Extracts Using Polyamide Minicolumns. *Biochem. Mol. Boil. Int.* **1998**, *45*, 791–796. [CrossRef]
20. Quideau, S.; Deffieux, D.; Douat, C.; Pouységu, L. Plant Polyphenols: Chemical Properties, Biological Activities, and Synthesis. *Angew. Chem. Int. Ed.* **2011**, *50*, 586–621. [CrossRef]
21. Zhang, P.-Y.; Yang, H.; Xu, Z.-L.; Wei, Y.-M.; Guo, J.-L.; Chen, D.-G. Characterization and Preparation of Poly (Vinylidene Fluoride) (PVDF) Microporous Membranes with Interconnected Bicontinuous Structures via Non-Solvent Induced Phase Separation (NIPS). *J. Polym. Res.* **2013**, *20*. [CrossRef]
22. Rahimpour, A.; Madaeni, S.; Zereshki, S.; Mansourpanah, Y. Preparation and Characterization of Modified Nano-Porous PVDF Membrane with High Antifouling Property Using UV Photo-Grafting. *Appl. Surf. Sci.* **2009**, *255*, 7455–7461. [CrossRef]
23. Wei, Q.; Zhang, F.; Li, J.; Li, B.; Zhao, C. Oxidant-Induced Dopamine Polymerization for Multifunctional Coatings. *Polym. Chem.* **2010**, *1*, 1430–1433. [CrossRef]
24. Al Aani, S.; Haroutounian, A.; Wright, C.J.; Hilal, N. Thin Film Nanocomposite (TFN) Membranes Modified with Polydopamine Coated Metals/Carbon-Nanostructures for Desalination Applications. *Desalination* **2018**, *427*, 60–74. [CrossRef]
25. Zhang, S.; Wu, L.; Deng, F.; Zhao, D.; Zhang, C.; Zhang, C. Hydrophilic Modification of PVDF Porous Membrane via a Simple Dip-Coating Method in Plant Tannin Solution. *RSC Adv.* **2016**, *6*, 71287–71294. [CrossRef]
26. Liu, C.; Wu, L.; Zhang, C.; Chen, W.; Luo, S. Surface Hydrophilic Modification of PVDF Membranes by Trace Amounts of Tannin and Polyethyleneimine. *Appl. Surf. Sci.* **2018**, *457*, 695–704. [CrossRef]
27. Poncet-Legrand, C.; Cabane, B.; Bautista-Ortín, A.-B.; Carrillo, S.; Fulcrand, H.; Pérez, J.; Vernhet, A. Tannin Oxidation: Intra- versus Intermolecular Reactions. *Biomacromolecules* **2010**, *11*, 2376–2386. [CrossRef]
28. Zhou, S.-K.; Liu, Y.-J.; Jiang, H.-Y.; Deng, W.-J.; Zeng, G.-M. Adsorption of U(VI) from Aqueous Solution by a Novel Chelating Adsorbent Functionalized with Amine Groups: Equilibrium, Kinetic, and Thermodynamic Studies. *Environ. Eng. Sci.* **2017**, *35*, 53–61. [CrossRef]
29. Vafajoo, L.; Cheraghi, R.; Dabbagh, R.; McKay, G. Removal of Cobalt (II) Ions from Aqueous Solutions Utilizing the Pre-Treated 2-Hypnea Valentiae Algae: Equilibrium, Thermodynamic, and Dynamic Studies. *Chem. Eng. J.* **2018**, *331*, 39–47. [CrossRef]
30. Tsai, S.-C.; Wang, T.-H.; Wei, Y.-Y.; Yeh, W.-C.; Jan, Y.-L.; Teng, S.-P. Kinetics of Cs Adsorption/Desorption on Granite by a Pseudo First Order Reaction Model. *J. Radioanal. Nucl. Chem.* **2008**, *275*, 555–562. [CrossRef]
31. Yuh-Shan, H. Citation Review of Lagergren Kinetic Rate Equation on Adsorption Reactions. *Scientometrics* **2004**, *59*, 171–177. [CrossRef]
32. Ho, Y.; McKay, G. The Sorption of Lead (II) Ions on Peat. *Water Res.* **1999**, *33*, 578–584. [CrossRef]
33. Salvestrini, S.; Vanore, P.; Bogush, A.; Mayadevi, S.; Campos, L.C. Sorption of Metaldehyde Using Granular Activated Carbon. *J. Water Reuse Desalination* **2016**, *7*, 280–287. [CrossRef]
34. Fenti, A.; Iovino, P.; Salvestrini, S. Some Remarks On "A Critical Review of the Estimation of the Thermodynamic Parameters on Adsorption Equilibria. Wrong Use of Equilibrium Constant in the Can't Hoof Equation for Calculation of Thermodynamic Parameters of Adsorption. *J. Mol. Liq.* **2019**, *276*, 529–530. [CrossRef]